Time-Multiplexed Measurements of Nonclassical Light at Telecom Wavelengths

G. Harder,[1] C. Silberhorn,[1,2] J. Rehacek,[3] Z. Hradil,[3] L. Motka,[3] B. Stoklasa,[3] and L. L. Sánchez-Soto[4,2]

[1]*Department of Physics, University of Paderborn, Warburger Straße 100, 33098 Paderborn, Germany*
[2]*Max-Planck-Institut für die Physik des Lichts, Günther-Scharowsky-Straße 1, Bau 24, 91058 Erlangen, Germany*
[3]*Department of Optics, Palacky University, 17. listopadu 12, 77146 Olomouc, Czech Republic*
[4]*Departamento de Óptica, Facultad de Física, Universidad Complutense, 28040 Madrid, Spain*

We report the experimental reconstruction of the statistical properties of an ultrafast pulsed type-II parametric down conversion source in a periodically poled KTP waveguide at telecom wavelengths, with almost perfect photon-number correlations. We used a photon-number-resolving time-multiplexed detector based on a fiber-optical setup and a pair of avalanche photodiodes. By resorting to a germane data-pattern tomography, we assess the properties of the nonclassical light states states with unprecedented precision.

PACS numbers: 03.65.Wj, 42.50.Ar, 42.50.Dv,42.65.Wi

arXiv:1406.3590v1 [quant-ph] 13 Jun 2014

Introduction.— Nonclassical states of light constitute an invaluable resource for deploying quantum-enhanced technologies as diverse as cryptography, computing, and metrology, to cite only some of the many relevant examples. Certifying signatures of nonclassicality generally requires inferring either the photon-number distribution or a quasiprobability distribution indirectly from a set of measurements. Even though the latter approach is well established [1] (it involves homodyne detection followed by an appropriate reconstruction scheme), photon counting seems a more natural choice in this discrete-variable scenario, in which photons are used as flying qubits.

However, capitalizing on photon counting places stringent demands on detector performance, quantified in terms of, e.g., spectral range, efficiency, dead time, dark-count rates, and timing jitter. This is currently driving considerable improvements in single-photon detectors [2–10]; in particular, the photon-number resolving (PNR) capability is nowadays required in most advanced protocols.

Several strategies have been proposed thus far for PNR detectors. Single-photon avalanche diodes (SPADs) have become the prevailing option for PNR applications. Si-based SPADs constitute a relatively mature technology with several efficient devices commercially available, but they are only suitable for use at visible and near infrared wavelengths. For experiments at technologically-important telecom wavelengths, the main contending technologies are InGaAs SPADs, which are plagued by high dark-count rates and long dead times, thereby making gating essential.

A proposal to employ a time-multiplexed detection (TMD) based on SPAD has been put recently forward [11–13]. These TMDs work also for pulsed light, and the photon-number distribution of a quantum state can be retrieved by inverting the measured photon statistics. Experimental applications, demonstrating a reliable loss calibration, and the TMD suitability for detecting multimode statistics and nonclassicality, have already been accomplished [14–19].

The effective implementation of these advanced schemes relies on a complete and accurate knowledge of the detector, an issue that has lately started to attract a good deal of attention [20–26]. The idea behind is to employ the outcome statistics in response to a set of complete certified input states.

However, as shown in Ref. [27], if the measurement itself is of no interest, the costly detector calibration can be bypassed by using a direct fitting of data in terms of detector responses to input probes. Thus, state estimation is done without any prior knowledge of the measurement, avoiding unnecessary wasting of resources on evaluating the parameters of the setup [28, 29].

In this Letter, we present a thorough application of this novel data-pattern tomography to TMDs. In this way, we provide a full account of the nonclassical properties of quantum states.

Experimental setup.— The states in our experiment are generated by type II parametric down conversion (PDC) inside a periodically poled KTP waveguide. The PDC source produces decorrelated signal and idler states with a purity for heralded states above 80% and high coupling efficiency into single-mode fibers. The setup is the same as the one described in detail in Ref. [30] and sketched in Fig. 1.

Twin beams created in PDC are archetypal example of highly correlated quantum states. Sub- and super-Poissonian photon statistics [31], antibunching [32], and quantum correlated quadrature amplitudes [33] have been demonstrated.

Our TMD is also schematized in Fig. 1. Two incoming pulses are split into 16 temporal bins and impinge onto SPADs. Counting the clicks allows us to estimate photon numbers and photon-number correlations between the two input ports. Since we work at telecom wavelengths, we use InGaAs SPADs (Id Quantique id201 at a repetition rate of 1 MHz with a gate width of about 2.5 ns). As briefly mentioned before, InGaAs SPADs SPADs are the simplest and most cost-efficient detectors available at telecom wavelengths. However, they have some disadvantages: the detection efficiencies are below 25% and afterpulsing is present with a few percent probability [34]. Consequently, the conventional TMD model [11], which only takes into account the probabilistic splitting and overall losses, appears to be inadequate. A more sophisticated technique is required to recover photon statistics from the measured click frequencies; this is where data-pattern tomography comes into play.

The state is specified by the two-mode photon-number distribution P_{mn}, where the first (second) index refers to the signal

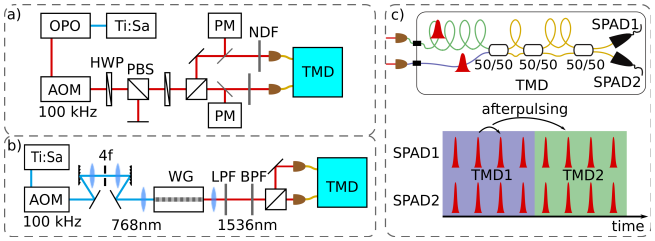

FIG. 1. (Color online) Left panel: (a) Probe-state generation. Pulsed light at telecom wavelengths is generated in a Ti:Sapphire pumped optical parametric oscillator (OPO). The repetition rate of the reference is lowered by an acousto-optical modulator (AOM). Motorized half-wave plates (HWP) followed by polarizing beam splitters (PBS) are used to vary the attenuation. The light power is measured by power meters (PM), further attenuated by neutral density filters (NDF), and coupled into the single-mode fibers of the time-multiplexing detector (TMD). (b) Nonclassical state generation. The pump light is spectrally tailored by a $4f$ system, coupled into the KTP waveguide (WG) and blocked by a long pass filter. The PDC photons pass a bandpass filter (BPF), are separated by a PBS and coupled into the TMD. Right panel: TMD. Two input pulses are distributed into 16 bins to obtain information about the photon number in each input as well as photon number correlations between the beams.

(idler) mode. We also denote by $p_{\alpha\beta}$ the probability of simultaneous signal (α) and idler (β) detection. Detections are thus described by 8-digit binary numbers, where 0/1 values mean click/no click in the corresponding time bin. For example, $\beta = 00000011$ denotes a simultaneous detection in the first two idler time bins. This gives $2^8 = 256$ distinct single-mode events and $2^{16} = 65536$ two-mode events to reckon with.

We adopt a linear model of the TMD detection, so that

$$p_{\alpha\beta} = \sum_{m=0}^{d-1}\sum_{n=0}^{d-1} C_{\alpha\beta,mn}\, P_{mn}\,, \tag{1}$$

where d is the cutoff dimension required to accommodate the relevant parts of the signal and the idler and the measurement matrix C provides a complete description of the TMD, including losses, detector efficiencies and afterpulsing effects.

In a real experiment, we acquire the relative frequencies $f_{\alpha\beta}$ after N random samples drawn from the multinomial distribution parametrized by $p_{\alpha\beta}$. Due to afterpulsing, it is not possible to factorize the detection matrix in signal and idler parts.

We also consider single-mode and heralded events; the former (latter) are simply marginal (conditional) probabilities of $p_{\alpha\beta}$. For these single-mode events, we look at the total number of clicks (either in the signal or the idler), without paying attention to the particular ordering of time bins. For example, for the signal-mode reconstruction, such reduction is readily done by summing data and patterns marginals $f_\alpha = \sum_\beta f_{\alpha\beta}$ over the $8!/[(8-k)!k!]$ different permutations of α with the same number k of nonzero binary digits.

Fitting data patterns.— From the measured data $f_{\alpha\beta}$ we have to determine the state P_{mn}. The standard detector tomography would proceed in two steps: first, a detector estimation, where the measurement matrix $C_{\alpha\beta,mn} \geq 0$ is inferred from a set of calibration states. Afterwards, the state $P_{mn} \geq 0$ is reconstructed from the previously obtained detector matrix. However, this is not completely satisfactory: the details of the TMD are not of interest and, besides, the detector estimation is exceedingly costly, scaling as d^4, which makes the method impractical, even for moderate values of this cutoff d.

The alternative data-pattern approach, we adopt here, expresses P_{mn} as a mixture

$$P_{mn} = \sum_{\xi=1}^{M} x_\xi\, P_{mn}^{(\xi)} = \sum_{\xi=1}^{M} x_\xi\, P_m^{(\xi)}\, P_n^{(\xi)}\,, \tag{2}$$

of M linearly independent (generally, nonorthogonal) two-mode coherent probes $\{P_{mn}^{(\xi)}\}$, with positive and negative weights $\{x_\xi\}$. This discrete representation can be thought of as a kind of generalization of the P-representation and can be sufficiently accurate depending on the number of terms in the sum.

The responses $f_{\alpha\beta}^{(\xi)}$ of the TMD to these coherent probes are called patterns. Then, by linearity, the data (i.e., the TMD response $f_{\alpha\beta}$ to an unknown state P_{mn}) can be modeled in terms of patterns as

$$f_{\alpha\beta} \simeq \sum_{\xi=1}^{M} x_\xi\, f_{\alpha\beta}^{(\xi)}\,. \tag{3}$$

Hence, once the patterns and data are measured, the coefficients x_ξ can be inferred from Eq. (3) and the state reconstructed according to (2). To this end, a suitable convex measure of the distance between the left- and right-hand side of Eq. (3) has to be minimized, subject to the physical constraints $P_{mn} \geq 0$ and $\sum_{mn} P_{mn} = 1$: this is a quadratic program than can be efficiently solved [35].

Notice that in the data-pattern tomography, the number of parameters $M-1$ is independent of the probe cutoff dimension d. Also, if needed, a partial tomography of the unknown state can be performed by using only a small part of the patterns or any linear function of them (such as the value of the Wigner function at the origin) for the data fitting in Eq. (3).

To create the probe states we use pulsed coherent light attenuated at the single-photon level. The power of the reference beam is changed by two motorized half-wave plates followed by polarizing beam splitters. We calibrate all the neutral density filters separately and measure fiber-coupling losses. From these values and the measured reference power, we calculate the power inside the fibers of the TMD. Due to the high degree of attenuation (of the order of 10^{-9}), small calibration errors (of order of a few percent) cannot be avoided. However, this affects the total losses, but not the shape of the photon statistics.

Results.— We take into consideration a fixed number of patterns with amplitudes below a given threshold $\alpha_{\max} \approx 2$. This threshold is important because of the afterpulsing, which

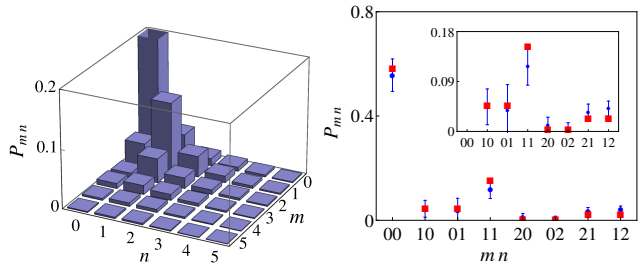

FIG. 2. (Color online) Two-mode reconstruction of the PDC_2 state. Left panel: Complete photon-number distribution, with $M = 50$ probes. Right: Comparison with the theoretical model. Circles with error bars represent the experimental results, whereas theory is indicated by squares.

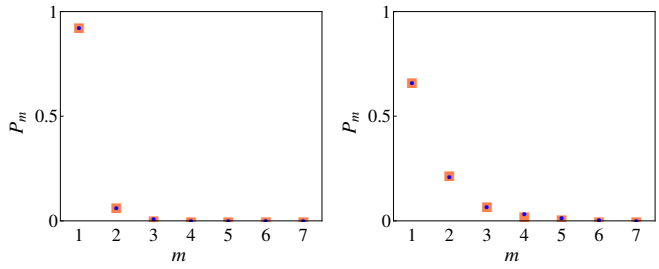

FIG. 3. (Color online) Single-mode signal reconstructions (dots) of PDC_1 (left) and PDC_2 (right), both with $M = 30$ probes. Best fits to Bose-Einstain distributions (squares) are also shown. The reconstruction errors are almost negligible and cannot be appreciated.

seems to be more pronounced for stronger states. The reconstruction is repeated 100 times with randomly chosen probe subsets of size $M < 235$ and averaged over those repetitions. In this way the redundancy in the data is propagated into the final estimate.

The variation within the set of reconstructions is used to estimate the associated errors, much in the spirit of nonparametric bootstrap [36]. In the experiment, $N_\xi = 4.2 \times 10^6$ events were registered for each coherent probe and PDC state. For low-intensity PDC states, the data were averaged over five repeated data acquisitions, making a total of $N_{\rm PDC} = 21 \times 10^6$ events. With these numbers, the statistical noise is insignificant (except, perhaps, for heralded detections) and the reconstruction accuracy is governed by systematic errors and afterpulsing effects.

To check the performance for different parameter sets we first performed a cross-validation [37], to verify whether the estimated state is consistent with the observed data sample. To this end, we checked the quality of the reconstruction with random sets of coherent states discarded from the probes, but with the same amplitude threshold. We have resorted to different measures of errors; for all of them we conclude that the accuracy is insensitive to the dimension d, while the errors get larger for stronger probes. Typical fidelities around 99% are attained, which amounts to errors of a few percent for the reconstructed elements of P_{mn}, which outperforms the standard detector tomography.

More probes give somewhat better results, but small sets of probes can be surprisingly good. This is due to the small variation across those patterns characterized by a small number of principal components in the singular value decomposition.

To compare with the theory, we assume the PDC distribution

$$\mathscr{P}_{mn} = \frac{\langle n\rangle^n}{(1+\langle n\rangle)^{1+n}}\,\delta_{mn}\,, \tag{4}$$

together a finite detection efficiency η which is taken into account by a Bernoulli distribution:

$$P_{mn} = \sum_{k=m}^{\infty}\sum_{\ell=n}^{\infty}\binom{k}{m}\binom{\ell}{n}\eta^{n+m}(1-\eta)^{k+\ell-n-m}\mathscr{P}_{k\ell}\,. \tag{5}$$

From the zero-detection probabilities of coherent probes with known amplitudes, the quantum efficiency of detectors was estimated to be 0.22 ± 0.01 and the coupling efficiency 75%. This, in turn, enables to calculate the mean photon numbers of the generated PDC states. Three PDC, denoted PDC_1, PDC_2 and PDC_3, were generated, with $\langle n_1\rangle = 0.11$, $\langle n_2\rangle = 0.76$, and $\langle n_3\rangle = 1.34$, respectively. These numbers were used to predict the two-mode statistics through Eqs. (4) and (5).

In Fig. 2 we plot typical results of two-mode TMD measurements for PDC_2. Strong signal-Idler correlations are observed and the agreement with the theory is pretty good. Similar results are found for other intensities.

In Fig. 3 we show the reconstructions of the signal states for two different pump intensities. Best fits to Bose-Einstein distributions are almost indistinguishable from the experimental results.

Heralded states are created by having the idler state conditioned on single or double detection in the signal of the PDC output. By double detection we mean here a click at detector A accompanied by a simultaneous click at detector B. Double detections at any single detector are discarded to avoid doubles caused by afterpulsing.

Heralded single- and especially two-photon states are difficult to reconstruct, since we are picking out quite a small subset of all the detection events. Besides, afterpulsing creates artificial signal-idler correlations, whose strength depends on the distance of the signal detection from the first idler time bin. All in all, this leads to larger reconstruction errors compared to single-mode states.

Reconstructed single-and two-photon heralded idler states from two different PDC states are shown in Fig. 4. To get theoretical predictions, we again assume an inefficient coupling (0.75) of the PDC state and calculate the post-measurement idler state P_i from the pre-measurement P as follows

$$P_i = \frac{{\rm Tr}_s(E\,P\,E^\dagger)}{{\rm Tr}_{s,i}(E\,P\,E^\dagger)}, \tag{6}$$

where $\hat{E}^\dagger\hat{E}$ is the POVM element describing the single/double detection in the signal mode and ${\rm Tr}_{s,i}$ indicates trace over the signal/idler. All states and POVM elements are diagonal here.

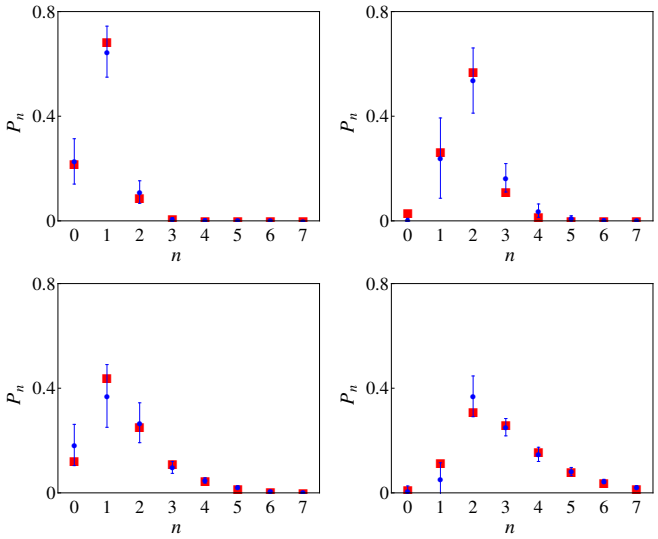

FIG. 4. (Color online) Reconstructed single-photon (left) and two-photon (right) heralded idler states generated from PDC_1 (top) and PDC_2 (bottom), with $M = 80$ probes. Squares denote again the corresponding theoretical predictions.

Best estimates of Wigner function at the origin for the single-photon heralded states are $W(0) = -0.72 \pm 0.06$ (PDC_1) and $W(0) = -0.30 \pm 0.09$ (PDC_2). This agrees with the calculated values $W(0) = -0.77$ (PDC_1) and $W(0) = -0.29$ (PDC_2), respectively and confirms the noclassicality of these states. With more intense PDC inputs, single detection in the signal tends to leave a mixture of Fock states in the idler. This explains why the nonclassicality of heralded states decreases with increasing pump intensity.

Finally, we simulated heralded states as post-measurement states based on the results of full two-mode tomography. To this end, we performed 100 two-mode reconstructions for each measured PDC state. The idler post-measurement state is calculated based on a thought single or double signal detection. The statistics of the resulting ensemble of heralded states is shown in Fig. 5, where we compare this statistics with the theoretical predictions.

These predictions based on the full two-mode reconstructions are less accurate than the single-mode heralded ones. The latter is more direct. In heralded detections, what helps is that the dimension of the search space is reduced and the dominating vacuum or even single-photon terms are eliminated, which improves the accuracy. In addition, in the data-pattern approach we use heralded coherent probes i.e. do the same data selection as for the PDC data. In this way, one somehow eliminates the artificial correlations created by the afterpulsing. Nevertheless, it is nice to see that the accord between single- and two-mode measurements is actually pretty good. One can also notice that the two-mode predictions improve with increasing intensity, as one could expect. More intense PDC states have larger higher-order P_{mn} components, which are easier to extract.

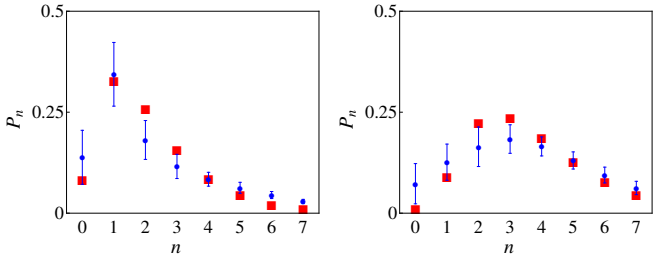

FIG. 5. (Color online) Heralded single-photon (left) and double-photon (right) Idler states as predicted from the reconstructed two-mode photon-number distributions of PDC_3, with $M = 80$ probes.

Concluding remarks.— In summary, we have exploited a PDC source of quantum states at telecom wavelengths with remarkable properties in terms of brightness, purity and symmetry. To put forward the nonclassical issues of the generated states, we have employed TMDs together with the method of data-pattern tomography. The experimental calibration shown here goes beyond any quantum detector tomography previously demonstrated. Our approach is easily adapted to a variety of measurement devices and the experimental implementation presented here shows its viability for complex detectors.

J. R., Z. H, L. M., and B. S. thank the financial assistance of the Technology Agency of the Czech Republic (Grant TE01020229) and the IGA Project of the Palacký University (Grant PRF 2013 019). L. L. S. S acknowledges the support from the Spanish MINECO (Grant FIS2011-26786).

[1] A. I. Lvovsky and M. G. Raymer, Rev. Mod. Phys. **81**, 299 (2009).
[2] R. H. Hadfield, Nat. Photon, **3**, 696 (2009).
[3] G. S. Buller and R. J. Collins, Meas. Sci. Technol. **21**, 012002 (2010).
[4] M. D. Eisaman, J. Fan, A. Migdall, and S. V. Polyakov, Rev. Sci. Instrum. **82**, 071101 (2011).
[5] J. P. Sprengers, A. Gaggero, D. Sahin, S. Jahanmirinejad, G. Frucci, F. Mattioli, R. Leoni, J. Beetz, M. Lermer, M. Kamp, S. Höfling, R. Sanjines, and A. Fiore, Appl. Phys. Lett. **99**, 181110 (2011).
[6] C. M. Natarajan, M. G. Tanner, and R. H. Hadfield, Supercond. Sci. Technol. **25**, 063001 (2012).
[7] W. H. P. Pernice, C. Schuck, O. Minaeva, M. Li, G. N. Goltsman, A. V. Sergienko, and H. X. Tang, Nat. Commun. **3**, 1325 (2012).
[8] B. Calkins, P. L. Mennea, A. E. Lita, B. J. Metcalf, W. S. Kolthammer, A. Lamas-Linares, J. B. Spring, P. C. Humphreys, R. P. Mirin, J. C. Gates, P. G. R. Smith, I. A. Walmsley, T. Gerrits, and S. W. Nam, Opt. Express **21**, 22657 (2013).
[9] A. Migdall, S. V. Polyakov, J. Fan, and J. C. Bienfang, eds., *Single-photon Generation and Detection* (Academic Press, Oxford, 2013).
[10] C. M. Natarajan, L. Zhang, H. Coldenstrodt-Ronge, G. Donati, S. N. Dorenbos, V. Zwiller, I. A. Walmsley, and R. H. Hadfield, Opt. Express **21**, 893 (2013).

[11] D. Achilles, C. Silberhorn, C. Śliwa, K. Banaszek, and I. A. Walmsley, Opt. Lett. **28**, 2387 (2003).

[12] J. Řeháček, Z. Hradil, O. Haderka, J. Peřina, and M. Hamar, Phys. Rev. A **67**, 061801 (2003).

[13] M. J. Fitch, B. C. Jacobs, T. B. Pittman, and J. D. Franson, Phys. Rev. A **68**, 043814 (2003).

[14] D. Achilles, C. Silberhorn, and I. A. Walmsley, Phys. Rev. Lett. **97**, 043602 (2006).

[15] M. Avenhaus, H. B. Coldenstrodt-Ronge, K. Laiho, W. Mauerer, I. A. Walmsley, and C. Silberhorn, Phys. Rev. Lett. **101**, 053601 (2008).

[16] A. P. Worsley, H. B. Coldenstrodt-Ronge, J. S. Lundeen, P. J. Mosley, B. J. Smith, G. Puentes, N. Thomas-Peter, and I. A. Walmsley, Opt. Express **17**, 4397 (2009).

[17] M. Avenhaus, K. Laiho, M. V. Chekhova, and C. Silberhorn, Phys. Rev. Lett. **104**, 063602 (2010).

[18] K. Laiho, K. N. Cassemiro, D. Gross, and C. Silberhorn, Phys. Rev. Lett. **105**, 253603 (2010).

[19] T. J. Bartley, G. Donati, X.-M. Jin, A. Datta, M. Barbieri, and I. A. Walmsley, Phys. Rev. Lett. **110**, 173602 (2013).

[20] A. Luis and L. L. Sánchez-Soto, Phys. Rev. Lett. **83**, 3573 (1999).

[21] J. Fiurášek, Phys. Rev. A **64**, 024102 (2001).

[22] G. M. D'Ariano, L. Maccone, and P. Lo Presti, Phys. Rev. Lett. **93**, 250407 (2004).

[23] J. S. Lundeen, A. Feito, H. Coldenstrodt-Ronge, K. L. Pregnell, C. Silberhorn, T. C. Ralph, J. Eisert, M. B. Plenio, and I. A. Walmsley, Nat. Phys. **5**, 27 (2009).

[24] T. Amri, J. Laurat, and C. Fabre, Phys. Rev. Lett. **106**, 020502 (2011).

[25] L. Zhang, A. Datta, H. B. Coldenstrodt-Ronge, X.-M. Jin, J. Eisert, M. B. Plenio, and I. A. Walmsley, New J. Phys. **14**, 115005 (2012).

[26] G. Brida, L. Ciavarella, I. P. Degiovanni, M. Genovese, L. Lolli, M. G. Mingolla, F. Piacentini, M. Rajteri, E. Taralli, and M. G. A. Paris, New J. Phys. **14**, 085001 (2012).

[27] J. Řeháček, D. Mogilevtsev, and Z. Hradil, Phys. Rev. Lett. **105**, 01040 (2010).

[28] D. Mogilevtsev, A. Ignatenko, A. Maloshtan, B. Stoklasa, J. Rehacek, and Z. Hradil, New J. Phys. **15**, 025038 (2013).

[29] M. Cooper, M. Karpinski, and B. J. Smith, arxiv:1306.6431 (2013).

[30] G. Harder, V. Ansari, B. Brecht, T. Dirmeier, C. Marquardt, and C. Silberhorn, Opt. Express **21**, 13975 (2013).

[31] H. D. Riedmatten, V. Scarani, I. Marcikic, A. Acin, W. Tittel, H. Zbinden, and N. Gisin, J. Mod. Opt. **51**, 1637 (2004).

[32] M. Koashi, K. Kono, T. Hirano, and M. Matsuoka, Phys. Rev. Lett. **71**, 1164 (1993).

[33] J. G. Rarity, P. R. Tapster, J. A. Levenson, J. C. Garreau, I. Abram, J. Mertz, T. Debuisschert, A. Heidmann, C. Fabre, and E. Giacobino, Appl. Phys. B **55**, 250 (1992).

[34] Y. Kang, H. Lu, Y.-H. Lo, D. Bethune, and W. Risk, Appl. Phys. Lett. **83**, 2955 (2003).

[35] L. Motka, B. Stoklasa, J. Rehacek, Z. Hradil, V. Karasek, D. Mogilevtsev, G. Harder, C. Silberhorn, and L. L. Sánchez-Soto, Phys. Rev. A **89**, 054102 (2014).

[36] A. C. Davison and D. V. Hinkley, *Bootstrap Methods and their Application* (Cambridge University Press, Cambridge, 1997).

[37] D. Mogilevtsev, Z. Hradil, J. Rehacek, and V. S. Shchesnovich, Phys. Rev. Lett. **111**, 120403 (2013).